Hindawi Publishing Corporation
EURASIP Journal on Wireless Communications and Networking
Volume 2007, Article ID 28073, 10 pages
doi:10.1155/2007/28073

Research Article

Measurements of MIMO Indoor Channels at 1800 MHz with Multiple Indoor and Outdoor Base Stations

Laura García,[1] Niklas Jaldén,[2] Björn Lindmark,[2] Per Zetterberg,[2] and Leandro de Haro[1]

[1] *Departamento de Señales, Sistemas Y Radiocommunicaciones, Universidad Politécnica de Madrid (UPM), 28040 Madrid, Spain*
[2] *Signal Processing Lab, School of Electrical Engineering, Royal Institute of Technology (KTH), 100 44 Stockholm, Sweden*

Received 1 April 2006; Revised 5 November 2006; Accepted 17 December 2006

Recommended by Rodney A. Kennedy

This paper proposes several configurations for multiple base stations in indoor MIMO systems and compares their performance. The results are based on channel measurements realized with a MIMO testbed. The receiver was moved along several routes and floors on an office building. Both outdoor and indoor locations are considered for the transmitters or base stations, which allow the analysis of not only indoor but also outdoor-to-indoor environment. The use of 2 base stations with different system level combinations of the two is analyzed. We show that the 2×4 configuration with base station selection provides almost as good performance as a 4×4 full water-filling scheme when the 2 base stations are placed at different locations. Also the spatial correlation properties for the different configurations are analyzed and the importance of considering path loss when evaluating capacity is highlighted.

1. INTRODUCTION

The substantial increase in capacity made possible with the use of multiple antennas has led to a considerable interest in multiple-input multiple-output (MIMO) systems ever since the seminal paper of Telatar [1].

When designing algorithms and schemes for MIMO systems, several assumptions to simplify the study and evaluation are usually made, such as ideal antenna arrays and adequate richness of separated multipath. However, in order to be able to predict the performance of a MIMO system in a realistic scenario, either detailed propagation simulations or measurements in real environments are required. Thus, the interest in realizing new MIMO measurements to better characterize the channel is clear.

Regarding MIMO channel characterization, a current topic of discussion is the trade-off between received power and rich multipath. A high SNR, as in line of sight (LoS) situations, may imply a low degree of scattering and spatial diversity [2]. On the other hand, nonline of sight (NLoS) cases suffer from higher path losses and thus lower received power than LoS ones, which may involve lower capacity for similar measured scenarios [3]. It is known that both factors (power and multipath richness) contribute to ergodic capacity, but it is not clear how to characterize their impact and importance, depending on the environment. In most works, it is common to see normalization of the channel matrix $\mathbf{H}$ to the instantaneous received power (or fixed signal-to-noise ratio, SNR, at the receiver) [4]. This is equivalent to assuming ideal power control in the system, so the path loss effect is not included. In our opinion, it is also of interest to consider the channel path loss and its relation to the transmitter and receiver locations. In [5] the capacity for LoS and NLoS fixed indoor positions is compared with and without power normalization. In [6] the authors proposed the normalization of the MIMO channel based on the average received SNR for the whole route in an outdoor scenario, so a fixed transmitted power is assumed. Comparisons of different normalization methods and their analysis in different scenarios are currently open issues, which are addressed in this paper.

Many measurement campaigns aiming to characterize the MIMO channel have been reported in the literature (see [7] for a summary). Despite the remarkable effort in characterizing and measuring MIMO channels, most of the previous works focus on either the indoor or the outdoor case. However, the outdoor-to-indoor scenario has important applications for data transmission in third generation cellular systems, as well as wireless local area networks (WLANs). The user equipment may be indoor while the base station may be located on a rooftop. One of the few examples that

includes this type of scenario is [8], where a measurement campaign conducted to validate a channel model is presented. Both indoor and indoor-to-outdoor measurements are included in the study, mainly aiming to check the proper behavior of the channel model in different scenarios. In [9] measurements and data evaluation for an outdoor-to-indoor case are presented, where the work is focused on the statistical distribution of the signal and direction of arrival. A similar study is [10], which also includes outdoor scenarios and compares the angle and path distance distribution for both types of environments. Recently, capacity results for a corridor-type scenario with indoor and outdoor transmitter locations were investigated, including polarization diversity [11]. Although some preliminary studies of indoor-outdoor environments have been done, most of them focus on a specific scenario or do not consider multiple transmitter locations, and the capacity analysis is scarce. Moreover, most of the previous works consider a single BS in the MIMO system. Thus, a more complete capacity analysis is needed, with the aim of examining several options for the BS location and their configuration scheme at system level.

The objective in this paper is twofold: to investigate the use of multiple base stations in an indoor environment, and to contribute to a better characterization of the properties of outdoor-to-indoor propagation. In all cases, we have measured the channel matrix as a function of location. This allows us to study not only the statistical properties of the channel, but also how the coverage varies with the exact office environment. Channel matrix normalization assuming fixed transmitted power or fixed received SNR power was considered, in order to give a better insight into the effect of received power and available spatial diversity in the capacity. Several schemes with one or two base stations are also investigated, and the system improvement obtained when channel state information is available at the transmitter is also shown.

The paper is organized as follows. In Section 2, the MIMO system used to collect the measurement data is described, as well as the considered scenarios. In Section 3, the analysis of correlation properties for different scenarios is presented. Section 4 shows capacity results for different system level options when two base stations are considered and several locations are analyzed. Finally, the conclusions of the paper are presented in Section 5.

2. MEASUREMENT SETUP

A narrowband MIMO testbed, developed in the Department of Signals, Sensors and Systems, KTH, was employed to perform a measurement campaign for different scenarios. The obtained data were used to evaluate several parameters and characteristics of the MIMO channel. A general description of the measurement system and studied environments is given below.

2.1. Measurement system

The measured data were collected with a 4 by 8 DSP-based testbed, whose general architecture is depicted in Figure 1

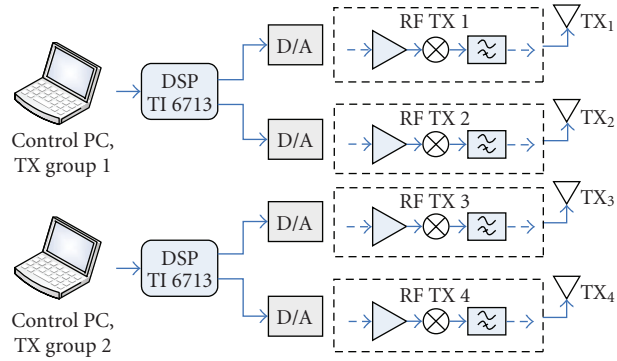

Figure 1: Illustration of the hardware transmitter modules. The radio frequency chains are schematically represented. Each Tx group has its own oscillator for frequency upconversion (not shown in the figure).

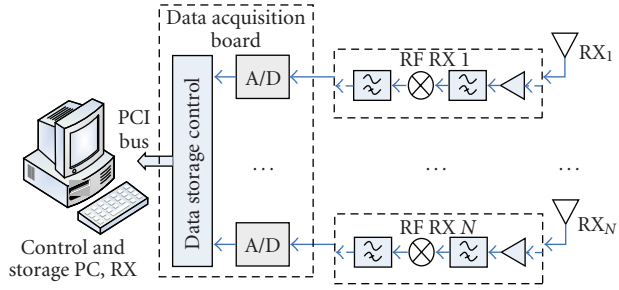

Figure 2: Illustration of the hardware receiver modules. The radio frequency chains are schematically represented. The same oscillator is used for frequency downconversion in all the Rx chains (not shown in the figure).

(transmitter modules) and Figure 2 (receiver modules). The testbed is a modified version of the one presented in [12]. It operates in an offline basis, so the received signal is first stored and after that postprocessed in a personal computer. The system bandwidth is 9.6 kHz, which allows narrowband channel measurements with high sensitivity. The offline and narrowband features simplify the system operation, since neither real-time constrains nor broadband equalization needs to be considered.

The carrier frequency is 1766.6 MHz. A heterodyne scheme with 2 intermediate frequencies is used, for both the transmitter and the receiver chains. For a thorough explanation of the radio frequency hardware, [13] may be consulted.

In order to study different transmitter configurations, the 4 transmitters were split into 2 groups of 2 transmitters each. The digital signals to be transmitted by each 2-Tx group were synchronously generated in a TI 6713 DSP, which was controlled by a laptop. The generated signals are digitally upconverted to the lower intermediate frequency, and after that analog-converted with a sampling rate of 48 ksps.

In the receiver side, the signal is analog-to-digital converted and then collected by a data acquisition board with up to 8 analog inputs, namely, the National Instruments

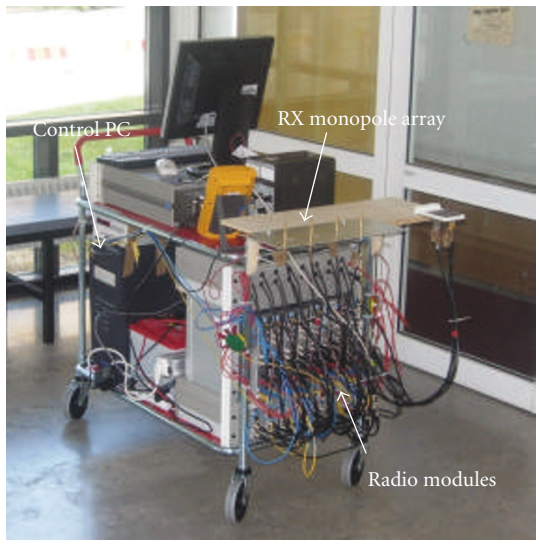

FIGURE 3: Receiver modules, mounted on a trolley to get a mobile station. A battery allowed 2 hours of stand alone power supply.

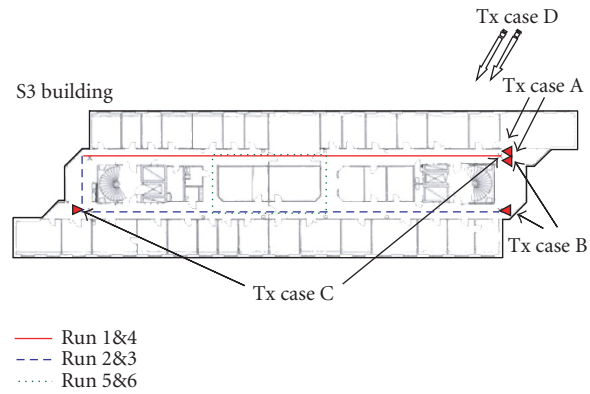

FIGURE 4: Floor plan (fourth floor) and locations for base stations 1 and 2 for the 4 cases in the measurement campaign.

NI-PCI6071E, with a sampling rate of 40 ksps. A dedicated PC is used to control the board and store the raw data. Afterwards, the files are postprocessed using Matlab^{TM}. The receiver modules are mounted on a trolley and powered by 12 V batteries to enable receiver mobility, so it may be carried along different routes. A photograph of the Rx modules is shown in Figure 3.

Finally, a calibration stage is performed to account for differences in the RF chains. The calibration values are obtained from back-to-back measurements on the testbed.

Regarding the antenna arrays, different options are considered in each link end. For the transmitter end, two Huber-Suhner dual-polarized planar antennas with slanted linear polarization ($\pm 45°$) are used for indoor locations A, B, and C (see below), while two powerwave broadband dual-polarized $\pm 45°$ antenna arrays are used for the outdoor location D. For the receiver end, two 4-element antenna arrays were designed and implemented. The first one is a conventional linear $\lambda/4$ monopole array with element spacing $d = \lambda/2$, which may be used as a reference array. The second one is a compact antenna array that consists of 4 PIFA elements. Since this paper focuses on the channel characterization for different transmitter locations, only the received signal from the monopole array will be considered thereafter (4×4 system). Details on the performance comparison from a point of view of MIMO system for the two arrays can be found in [14, 15].

2.2. Transmitted signals and channel estimation

A digital sine wave was chosen as a transmitted baseband signal for the measurements. A different frequency was used for each transmitter in order to be able to separately detect each transmitted signal in the receiver, and thus properly estimate all the elements in the channel matrix **H**. The used frequencies for the baseband sine waves were $f_{Tx1} = 1$ kHz, $f_{Tx2} = 0$ kHz, $f_{Tx3} = -1$ kHz, and $f_{Tx4} = -2$ kHz. Since very close frequencies were chosen, the frequency channel response can be considered flat in the whole measured bandwidth. Use of a simple sine wave instead of pseudonoise codes or more complex signals simplifies the required signal processing to estimate the channel matrix **H**, but it is still accurate to analyze the narrowband properties of the measured scenarios.

The estimation of the **H** matrix was performed by correlating the received signal with a complex exponential $\exp(j2\pi f t)$ for each transmitter. In order to account for possible frequency mismatch between transmitter and receiver or frequency drift in the oscillators during the measurement, the nominal baseband frequencies for the expected sine waves were not directly considered, but they were used to estimate the actual received frequencies for each sine wave. The previously computed calibration tables were then used to calibrate the estimated **H** matrix.

2.3. Measured environments

The measurement campaign was carried out in the S3 building and surroundings, in the KTH Campus. Several scenarios were included, with especial emphasis on the consideration of different locations and configurations for the transmitters. Figure 4 shows the layout of the fourth floor considered in this paper, the main routes traveled, as well as the 4 different transmitter positions: A, B, C, and D. These cases are summarized as follows.

(i) *Case A*: the 4 transmitter antennas (A12, A34) were located at one end of the fourth floor in the S3 building.

(ii) *Case B*: the transmitters were split into 2 groups (B12 and B34) or *base stations* (BSs) and each BS was placed spatially separated at the same end of the fourth floor in the S3 building.

(iii) *Case C*: the transmitters were split into 2 BS (C12 and C34) and each one was located at a different end of the fourth floor in the S3 building (maximal spatial separation).

(iv) *Case D*: the 4 transmitter antennas (D12, D34) were located at the flat roof of the Q building (in front of the S3

Figure 5: The S3 building from antennas viewpoint in outdoor location. The antennas are pointing approximately at the fourth floor, where some receiver routes were conducted.

building). The S3 building seen from the outdoor base station, case D, is shown in Figure 5.

We may note that case D consists in an outdoor-to-indoor environment, while the other cases are indoor environment. Thus, 2 different environment types are addressed in the measurement campaign.

The receiver was moved along the same indoor routes for all cases A–D at a pedestrian speed (approximately 0.9 m/s). The measurements included situations of line of sight (LoS) and nonline of sight (NLoS), as well as routes inside the offices. Three different floors in the building were covered with the measured routes.

Table 1 summarizes measurement setup characteristics for the considered environments.

Table 1: Main characteristics of measurement setup.

	Cases A, B, C	*Case D*
Tx location	Indoor	Outdoor
Tx power/branch	−5 dBm	25 dBm
Tx antenna elements spacing (for each BS)	0.6λ	6λ
Rx antennas spacing	0.5λ	
Polarization at Tx	Slanted ±45° linear	
Polarization at Rx	Vertical (linear)	
Carrier frequency	1766.6 MHz	
System BW	9.6 kHz	
Time resolution after channel estimation	0.01 s	
MS speed	0.9 m/s	
Number of Tx and Rx elements ($N_{\mathrm{Tx}} \times N_{\mathrm{Rx}}$)	4×4	

3. CORRELATION ANALYSIS

In order to evaluate the measured scenarios, some propagation characteristics were analyzed. From a point of view of MIMO system, the spatial correlation properties of the channel are of paramount importance. It has been shown in [8] that the spatial correlation matrices at the transmitter $\mathbf{R_{Tx}}$ and receiver $\mathbf{R_{Rx}}$ can be used to estimate the correlation matrix $\mathbf{R}$ of a MIMO system in some cases such as indoor NLoS, which in turn gives a direct insight into the achievable spatial diversity and MIMO capacity.

Let us consider an $N_{\mathrm{Tx}} \times N_{\mathrm{Rx}}$ MIMO system, N_{Tx} being the number of transmit antennas and N_{Rx} the number of receive antennas. The input-output relationship for a narrowband MIMO channel is expressed as

$$\mathbf{y} = \mathbf{H}\mathbf{x} + \mathbf{n}, \tag{1}$$

where $\mathbf{y}$ and $\mathbf{x}$ are the received and transmitted signals, respectively, and $\mathbf{n}$ is a vector of additive white Gaussian noise with variance σ^2. The channel matrix $\mathbf{H}$ consists of $N_{\mathrm{Rx}} \times N_{\mathrm{Tx}}$ elements, h_{ij}, which are the channel gains between transmitter j and receiver i.

When computing the spatial correlation coefficients between two antennas, two options may be considered: either the complex information is taken into account or else the phase is discarded and only the power (envelope) information is used. In the context of modeling, the complex correlation coefficient ρ^{cplx} is preferred, since it carries the full information (amplitude and phase) of the radio channel, which is required to properly combine the modeled multipath scenarios. However, the power correlation coefficients ρ^{pow} have a clearer engineering interpretation than the complex correlation coefficient, which makes them suitable for analyzing correlation properties of a measured MIMO channel. Since we are interested in the analysis of the signal, studying the power correlation is fair enough. Moreover, it has been shown in [16, 17] that both correlation coefficients are linked. In the case of Rayleigh distributed signals, their relationship is given by the following expression (see [18]):

$$\rho^{\mathrm{pow}} = \left|\rho^{\mathrm{cplx}}\right|^2. \tag{2}$$

For indoor environments (as the one analyzed in this work), we may assume multipath richness and Rayleigh distributed signals in general, so the expression above will hold in our case. For clarity reasons, we will hereafter refer to the power spatial correlation coefficient simply as correlation coefficient, ρ. We may note that the measured routes are mostly NLoS, thus (2) is applicable in most cases.

The correlation coefficient between transmitters i and j is then computed as

$$\rho_{i,j}^{\mathrm{pow,Tx}} = \left\langle \left|h_{m,i}\right|^2, \left|h_{m,j}\right|^2 \right\rangle, \tag{3}$$

where $\langle \cdot, \cdot \rangle$ denotes the correlation operation, defined as

$$\rho_{a,b} = \langle a, b \rangle = \frac{\mathrm{E}\{ab^*\} - \mathrm{E}\{a\}\mathrm{E}\{b^*\}}{\sqrt{\left(\mathrm{E}\{|a^2|\} - \left|\mathrm{E}\{a\}\right|^2\right)\left(\mathrm{E}\{|b|^2\} - \left|\mathrm{E}\{b\}\right|^2\right)}}, \tag{4}$$

where $\mathrm{E}\{\cdot\}$ denotes expectation and $(\cdot)^*$ is the conjugate operation. The slow fading is removed by local averaging of the power over a distance of 1 m.

Similarly, the spatial power correlation coefficient between receivers i and j is computed as

$$\rho_{i,j}^{\text{pow,Rx}} = \left\langle |h_{i,m}|^2, |h_{j,m}|^2 \right\rangle. \quad (5)$$

The correlation coefficients for each transmitter pair were computed for the 4 transmitter locations under study, considering all the measured routes. The computed cumulative distributed functions are depicted in Figure 6.

As expected, the correlation is much smaller when considering antennas in spatially separated base stations (cases B, C) than for cases where both base stations are closely located (cases A, B). The highest correlation scenario is found to be case A, where the mean correlation coefficients vary from 0.45 to 0.55. We may notice that in this case the polarization diversity in transmitters offers some interesting decorrelation, reducing the mean value of ρ from $\rho_{13} = 0.53$ to $\rho_{14} = 0.45$ and from $\rho_{24} = 0.53$ to $\rho_{23} = 0.5$.

When the base stations are spatially separated but in the same end of the office floors, as in case B, the correlation between antennas in different base stations is substantially reduced, due to the increase in spatial diversity obtained by separating the antennas. Moreover, the new location for the base stations causes that when one BS is received in LoS, the other one is received in NLoS, which also reduces correlation between base stations. The same effect holds for case C (base stations placed at opposite ends of the office floor), where the correlation is even lower. In this case, the antennas in different base stations are highly uncorrelated; the average ρ is close to 0.1 and there is a small variance around this value. Nevertheless, the use of different polarizations does not introduce extra decorrelation in these 2 cases, mainly due to the already low level of correlation.

When the outdoor location is considered for the transmitters (case D), a slightly lower correlation than in the indoor case (case A) is observed, which can be explained by the fact that the antenna groups were more closely located in case A ($d = \lambda/2$) than in case D ($d = 4.7\lambda$). However, it is quite interesting to notice that, compared to the case of indoor Tx location (case A), for the outdoor location, the extra decorrelation obtained by using dual-polarized antennas is more important than the one obtained due to spatial separation, even though the spacing is larger: while the lowest average correlation coefficient is obtained for antennas pairs with spatial and polarization diversities (1–4 and 2-3), the highest one is observed for antenna pairs with the same polarizations (1–3 and 2–4). Thus, lower polarization correlation was obtained for outdoor-to-indoor cases than for full indoor ones.

Regarding the spatial correlation at a receiver pair, the closer the elements are, the higher the correlation is ($\rho_{14} < \rho_{13} < \rho_{12}$ and so on), as expected (Figure 7). Similar statistical distributions of ρ are obtained for the four measured situations. Thus, only curves for case A are shown. However, it is interesting to notice that the average ρ value is found to be slightly smaller for the outdoor location (see Table 2), since there are less LoS (highly correlated) routes.

Knowing the spatial correlation at transmitter and receiver is useful to get an idea of possible available spatial diversity in the system. However, it may be of interest to consider the comparison of achievable capacity for each case. Moreover, it has been shown in [19] that in some cases, such as keyholes [20], low correlation at transmit and receive ends does not involve a high capacity. In order to complete the analysis, next section shows capacity results for the measured scenarios.

4. CAPACITY ANALYSIS

This section shows the capacity results obtained from the measured $\mathbf{H}$ matrices for different scenarios. Since capacity does not only depend on the multipath richness of the channel, but also on the signal-to-noise ratio (and thus received power), we will first study the path loss as a function of Rx position along the routes and of Tx location.

4.1. Path loss

Figure 8 shows the path loss as a function of location on the fourth floor for cases A–D. We define the path loss from the average channel coefficient:

$$\text{PL} = 10\log_{10}\left(\frac{1}{N_{\text{Tx}}N_{\text{Rx}}}\sum_{i,j}|h_{ij}|^2\right) \quad (6)$$

and the values shown in Figure 8 are the average in each square. Note that for cases B and C, we actually see the average path loss from one mobile location to two different base stations. The average path loss for the whole floor is shown in Table 3.

The path loss plots indicate that for a total transmitted power, the power is better distributed for cases where the base stations are not colocated (cases B and C), which seems reasonable. These cases provide more LoS situations (due to the propagation in the north and south hallways), and thus a better coverage.

4.2. Capacity results

To give a fair comparison between the studied scenarios, we have normalized the transmit power for the indoor cases A, B, and C so that the average SNR for case A over the whole floor is 10 dB. The transmit power is thus

$$P_{\text{ABC}} = \frac{N_{\text{Rx}}N_{\text{Tx}}\sigma^2\,\text{SNR}}{E\left\{\|\mathbf{H}_A\|_F^2\right\}}, \quad (7)$$

where $\|\cdot\|_F$ denotes the Frobenius norm. Since the path loss is much greater for the outdoor case, a separate normalization PD is used for case D, again resulting in an average SNR = 10 dB. Thus, we still take into account the different path loss to different locations and the effect of more or less even geographical coverage. For each scenario, the BS is assumed to transmit at full but fixed transmit power PABC, or PD regardless of the number of transmitter antennas. This leads to a variation in the received signal-to-noise ratio as the mobile moves along its trajectory. We then evaluate the capacity in b/s/Hz as [1]:

$$C = \log_2\left|\mathbf{I} + \mathbf{HQH}^*\right|, \quad (8)$$

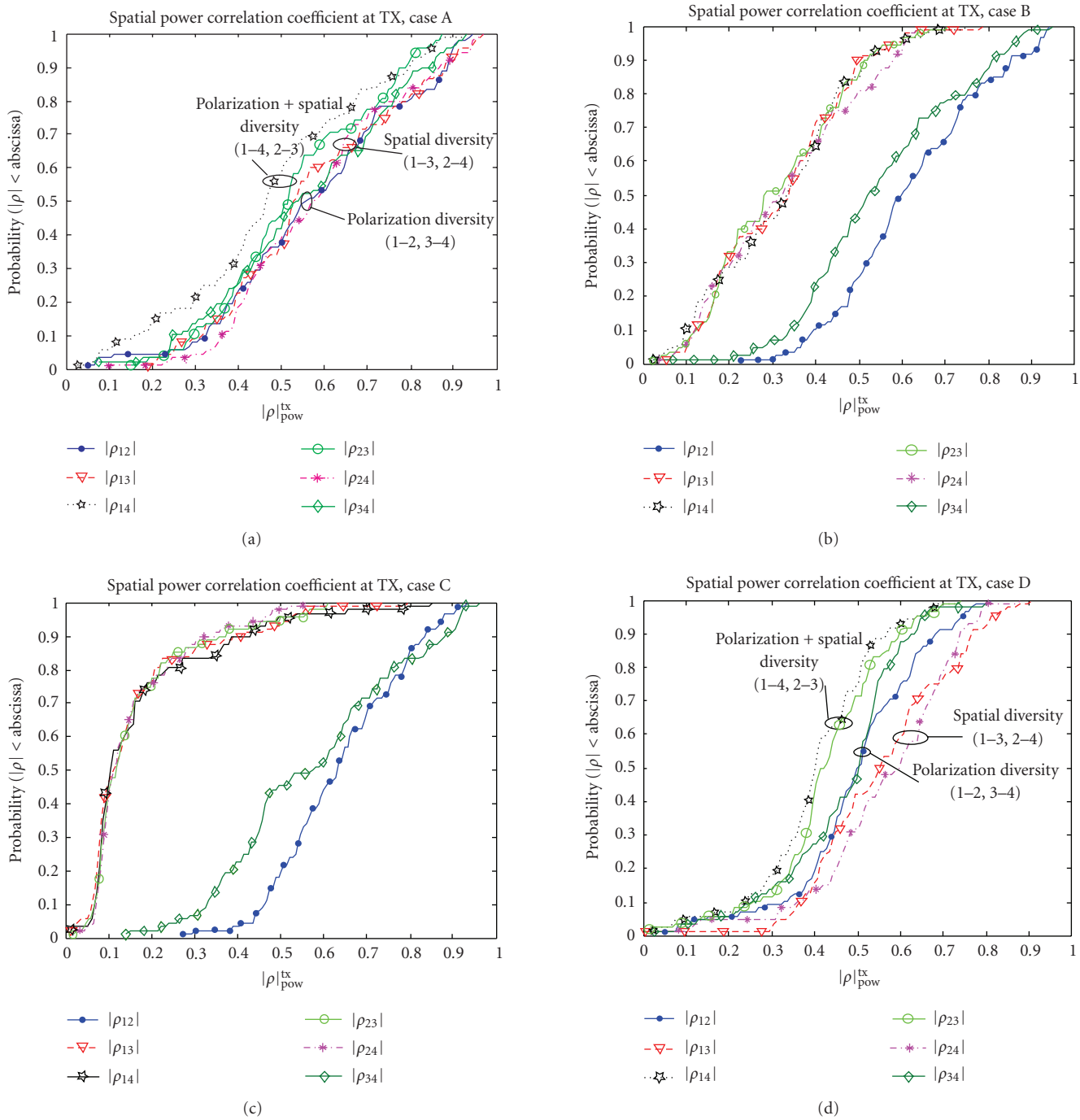

FIGURE 6: Empirical CDF of the power correlation coefficients for transmit antennas. Four locations are considered for the 2 base stations (with 2 dual-polarized antennas each): indoor colocation (a), indoor medium spatial separation (b), indoor opposite location with larger separation (c), and outdoor location (d). The receiver module is moved along 22 indoor routes. Very low transmitter correlation is obtained for cases with medium and large spatial separations. An interesting decrease in correlation is obtained for antennas with different polarizations for outdoor location.

where $\mathbf{Q}$ is the transmit covariance matrix such that $\mathrm{Tr}\{\mathbf{Q}\} = P_{\mathrm{ABC}}$ or P_{D}. To compare cases A–D, we consider the following options of signal processing at a system level.

(i) Option 1: no information is shared between the two BS and the mobile can only see one BS during the whole time. This will give the capacity for a 2×4 system. The BS has full channel state information (CSI) and allocates power to its antennas according to the water-filling scheme [21].

(ii) Option 2: no information is shared between the BS, but the MS makes a selection between the BS based on the strongest received power. This will give the capacity for a 2×4 system with BS selection. Both BS are assumed to have full

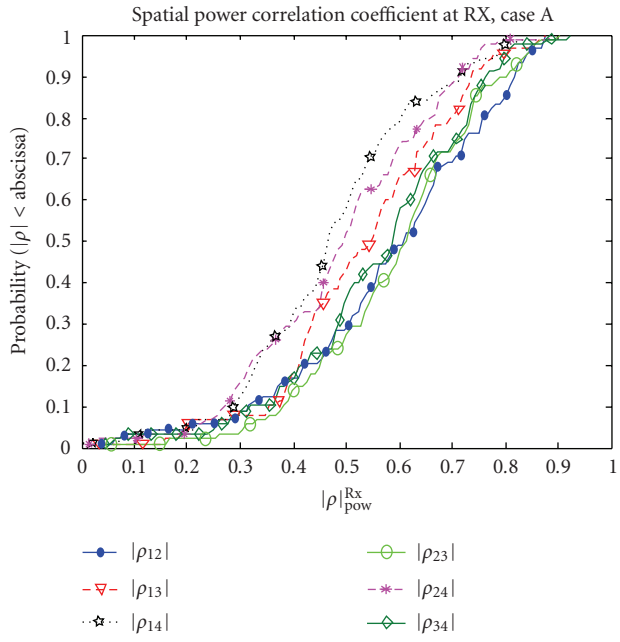

Figure 7: Empirical CDF of the power correlation coefficients for receive antennas. Only case A is shown, very similar results are obtained for the other three cases (B, C, and D).

Table 2: Average values of spatial correlation at receiver.

	Case A	Case B	Case C	Case D
Mean ρ^{Rx}	0.56	0.50	0.52	0.47

CSI and allocate power using water-filling scheme.

(iii) Option 3: both BS share all information and transmit powers. Full CSI is assumed and water-filling over the full 4×4 channel is calculated. The total available transmit power is P_{ABC} or P_{D} and the system is not limited to use half the power on each BS.

Options 1 and 2 are reasonable to assume for all measurement cases, while option 3 is probably only reasonable when both BS are closely located. However the third option is still interesting since it will serve as an upper bound on the achievable capacity for this setup.

Let us first study the variation of the capacity with location for cases A–D. Figure 9 shows the local average capacity including path loss effect for the hallways and some of the offices on the fourth floor. Thus, these plots can be interpreted as coverage plots for the MIMO system. Starting with case A, we have a very high capacity close to the base station, but a poor coverage in the south hallway.

Case B, on the other hand, provides a more even coverage since we get propagation along both hallways. We also see that option 2 (selection of 2×4) is practically equivalent to option 3, the full 4×4 system. The capacity drops below 10 b/s/Hz at approximately 20 m in both cases. Only in the open area around the BS (to the far right), where we can receive substantial power from both BS, we do see a slight improvement using full water-filling. Taking into account that the full 4×4 system option requires that the 2 BS share the CSI at any moment, the 2×4 system with BS selection seems a very interesting solution.

Table 3: Average path loss for all measured routes (dB).

	Case A	Case B	Case C	Case D
Path Loss (dB)	59.2	56.9	53.9	83.15

Next, looking at case C, we see that we have the same range of coverage, $>$ 10 b/s/Hz up to 20 m, as case B. Also in this case, option 2 (selection) and option 3 (full 4×4 water-filling) yield almost identical capacity results. Again the difference is seen only in the far ends (right or left), where water-filling provides 2-3 bits higher capacity.

For case D we have used a separate normalization as mentioned above, equivalent to using 24 dB higher transmit power than the indoor cases. This gives a larger region that has capacity above 10 b/s/Hz, and we now cover the offices in the northern corridor. The coverage is more evenly distributed, but this is to the cost of higher transmit power.

Moving on to the capacity statistics, we first see in Figure 10 the CDF of the capacity for the whole floor for 2×4 systems with and without BS selection. The same power normalization is used as in Figure 9. The fixed systems represent single 2×4 systems with BS at the four different transmitter locations, shown in Figure 4. Judging from the symmetry of the fourth floor, we might expect identical capacity for the indoor cases A, B, and C. However, our choice of routes combined with unavoidable changes in the propagation conditions from measurement to measurement results in the slight difference seen in Figure 10.

Case D, compensated with a 24 dB higher power, is clearly superior. However with BS selection case C, is superior. This is due to the better power distribution over the whole floor and macro diversity gains. For cases A and D, there is only a slight improvement when using BS selection, due to a limited spatial diversity.

Next, Figure 11 shows the CDF of the capacity for option 3, a full 4×4 system, and option 2, selection between 2×4 systems. Cases B-C show no improvement using a full 4×4 system, indicating that the system will be making a selection of a 2×4 system. For cases A and D, we have a slight improvement attributed to beamforming gain and some spatial diversity (cf. Figure 6). The most important conclusion form Figure 11, however, is that 2×4 selection in cases B and C vastly outperforms the full 4×4 system of case A. Thus, for indoor base stations, we are much better of using separate 2×4 systems and simple selection compared to a single 4×4 system. The reason is due to both lower average path loss (cf. Table 3) and a lack of spatial gain due to the hallway propagation, see below.

Finally, we have studied the capacity for a fixed local average SNR to see how ideal our MIMO channel is. Figure 12 shows the CDF of the capacity with local SNR $=$ 10 dB averaged over a 1- m distance. We see both the case of water-filling assuming perfect CSI and the case of no CSI at the transmitter. The result shows that the outdoor case D provides the highest degree of multipath. With a fixed SNR

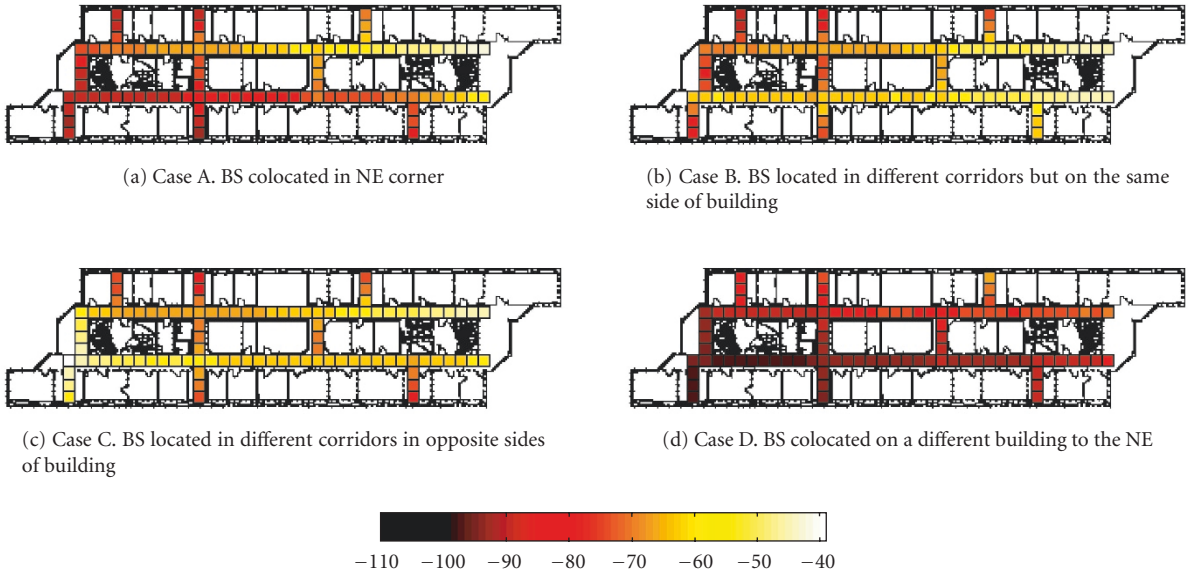

(a) Case A. BS colocated in NE corner

(b) Case B. BS located in different corridors but on the same side of building

(c) Case C. BS located in different corridors in opposite sides of building

(d) Case D. BS colocated on a different building to the NE

FIGURE 8: Average path loss $\sum_{ij} |h_{ij}|^2/N_{\mathrm{Tx}}/N_{\mathrm{Rx}}$ for cases A–D with different locations for base stations are presented.

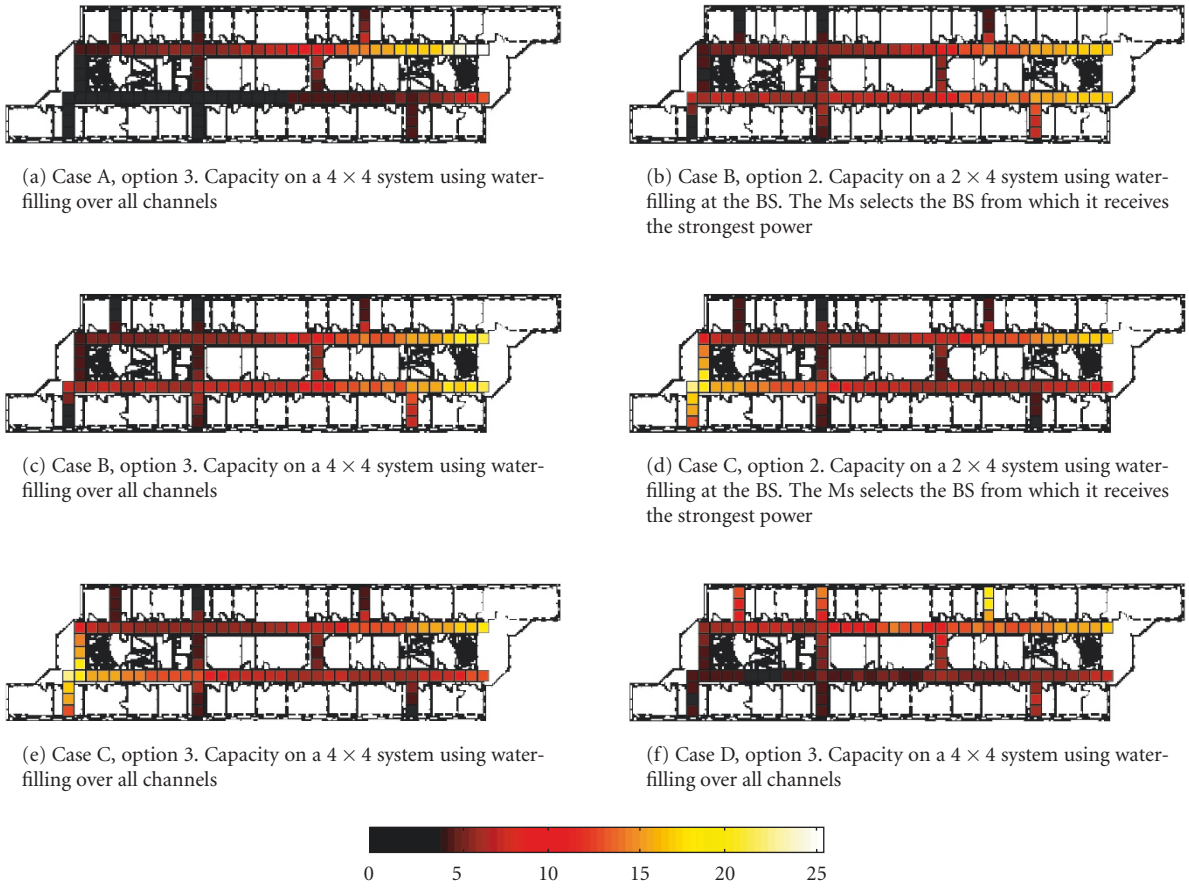

(a) Case A, option 3. Capacity on a 4×4 system using water-filling over all channels

(b) Case B, option 2. Capacity on a 2×4 system using water-filling at the BS. The Ms selects the BS from which it receives the strongest power

(c) Case B, option 3. Capacity on a 4×4 system using water-filling over all channels

(d) Case C, option 2. Capacity on a 2×4 system using water-filling at the BS. The Ms selects the BS from which it receives the strongest power

(e) Case C, option 3. Capacity on a 4×4 system using water-filling over all channels

(f) Case D, option 3. Capacity on a 4×4 system using water-filling over all channels

FIGURE 9: Capacity maps including path loss in the **H** matrices. The transmit power is chosen so that the average SNR = 10 dB for the whole floor, in the four studied cases.

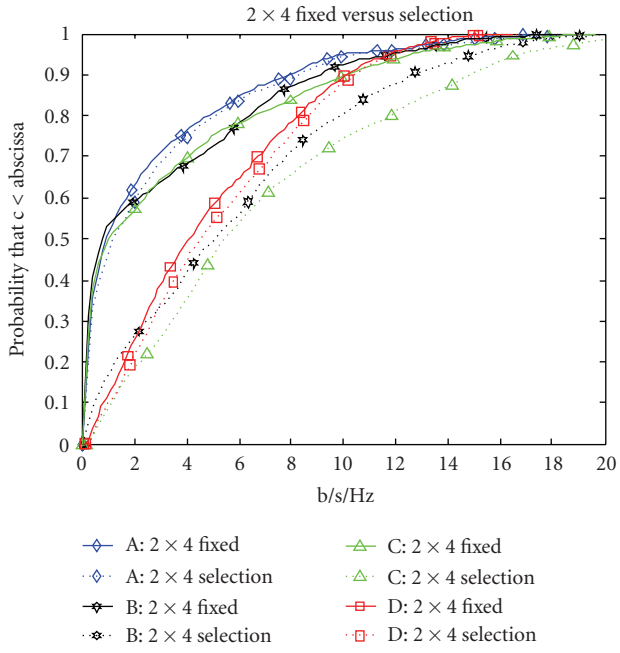

FIGURE 10: Capacity CDF for option 1 (a fixed 2 × 4 system) and option 2 (selection between two 2 × 4 systems).

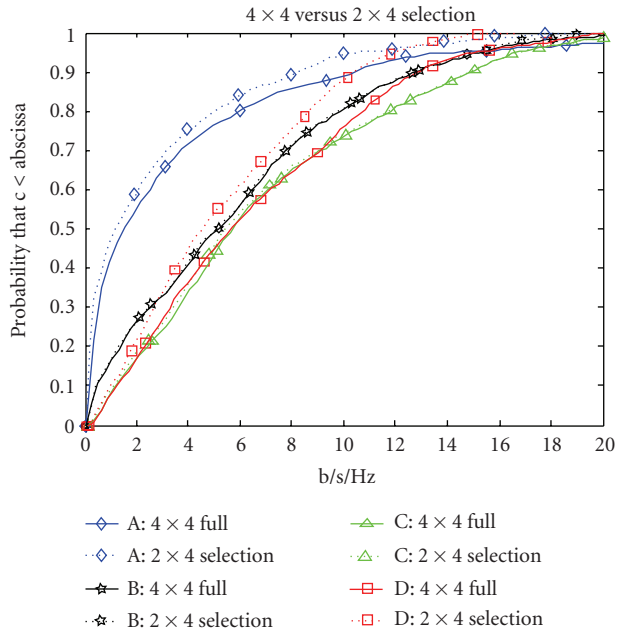

FIGURE 11: Capacity CDF for option 3 (full 4×4 system) and option 2 (selection between two 2 × 4 systems).

neglecting path loss, case A will also outperform cases B and C since the latter will have quite unequal eigen values due to different path loss to the two base stations. Compared with, for example, the mean capacity of 10.9 b/s/Hz for a 4×4 i.i.d. channel with no CSI, it is also clear that our channel is non-ideal.

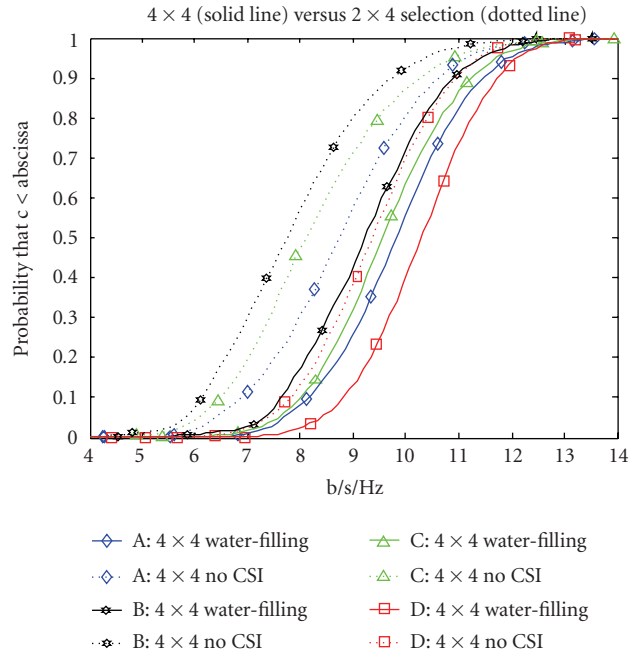

FIGURE 12: Comparison of water-filling (full CSI at Tx) and no CSI at Tx for a 4 × 4 MIMO case at a local average SNR = 10 dB.

5. CONCLUSION

Different transmitter locations and MIMO transmit schemes have been evaluated with respect to transmit correlation, path loss, and capacity. In particular, we have compared selection between two 2 × 4 MIMO systems and a full 4 × 4 system. Our results show that the BS selection scheme is the superior when the base stations are separated (option 2 of cases B and C). The reason is the more even signal coverage seen in Figure 8. For these cases, it is also clear that a full 4×4 system yields very marginal capacity increase because all the powers will still be distributed on a single BS.

Comparing cases A and D, we have shown that the outdoor-to-indoor case (D) provides lower correlation than the indoor one (A) with hallway propagation. This results in a higher capacity for case D if we ignore the effect of path loss and consider a fixed local average SNR (Figure 12). Note that for this scenario of normalized received SNR, the choice of a separated BS (cases B and C) provides lower capacity. This is the opposite from the result considering the effect of the path loss. Finally, we note that the indoor environment is not an ideal MIMO channel; the mean capacity is approximately 1.5 bits lower than the ideal at 10 dB SNR.

ACKNOWLEDGMENTS

This work was done as a collaboration in the Antenna Center of Excellence (FP6-IST 508009) within the EC 6th Framework Program. The authors wish to thank the reviewers for their helpful suggestions.

REFERENCES

[1] I. E. Telatar, "Capacity of multi-antenna Gaussian channels," Internal Technical Memo, AT&T Bell Laboratories, Murray Hill, NJ, USA, June 1995.

[2] T. Svantesson and J. Wallace, "On signal strength and multipath richness in multi-input multi-output systems," in *Proceedings of IEEE International Conference on Communications (ICC '03)*, vol. 4, pp. 2683–2687, Anchorage, Alaska, USA, May 2003.

[3] A. F. Molisch, M. Steinbauer, M. Toeltsch, E. Bonek, and R. S. Thomä, "Capacity of MIMO systems based on measured wireless channels," *IEEE Journal on Selected Areas in Communications*, vol. 20, no. 3, pp. 561–569, 2002.

[4] M. D. Batariere, T. K. Blankenship, J. F. Kepler, et al., "Wideband MIMO mobile impulse response measurements at 3.7 GHz," in *Proceedings of the 55th IEEE Vehicular Technology Conference (VTC '02)*, vol. 1, pp. 26–30, Birmingham, Ala, USA, May 2002.

[5] J. W. Wallace and M. A. Jensen, "Measured characteristics of the MIMO wireless channel," in *Proceedings of the 54th IEEE Vehicular Technology Conference (VTC '01)*, vol. 4, pp. 2038–2042, Atlantic City, NJ, USA, October 2001.

[6] T. Fügen, C. Kuhnert, J. Maurer, and W. Wiesbeck, "Performance of multiuser MIMO systems under realistic propagation conditions," in *Proceedings of ITG Workshop on Smart Antennas*, pp. 167–173, Munich, Germany, March 2004.

[7] L. Schumacher, L. T. Berger, and J. Ramiro-Moreno, "Recent advances in propagation characterisation and multiple antenna processing in the 3GPP framework," in *Proceedings of the 26th URSI General Assembly*, Maastricht, The Netherlands, August 2002.

[8] J. P. Kermoal, L. Schumacher, K. I. Pedersen, P. E. Mogensen, and F. Frederiksen, "A stochastic MIMO radio channel model with experimental validation," *IEEE Journal on Selected Areas in Communications*, vol. 20, no. 6, pp. 1211–1226, 2002.

[9] S. Wyne, P. Almers, G. Eriksson, J. Karedal, F. Tufvesson, and A. F. Molisch, "Outdoor to indoor office MIMO measurements at 5.2 GHz," in *Proceedings of the 60th IEEE Vehicular Technology Conference (VTC '04)*, vol. 1, pp. 101–105, Los Angeles, Calif, USA, September 2004.

[10] J. Medbo, M. Riback, H. Asplund, and J. Berg, "MIMO channel characteristics in a small macrocell measured at 5.25 GHz and 200 MHz bandwidth," in *Proceedings of the 62nd IEEE Vehicular Technology Conference (VTC '05)*, vol. 1, pp. 372–376, Dallas, Tex, USA, September 2005.

[11] L. García-García, C. Gómez-Calero, J. Mora-Cuevas, R. Martínez-Rodríguez-Osorio, and L. de Haro-Ariet, "Comparison of MIMO single and multi-polarized measured channels in indoor WLAN scenarios," in *Proceedings of the 1st European Conference on Antennas and Propagation (EuCAP '06)*, Nice, France, November 2006, (ESA SP-626).

[12] D. Samuelsson, J. Jaldén, P. Zetterberg, and B. Ottersten, "Realization of a spatially multiplexed MIMO system," *EURASIP Journal on Applied Signal Processing*, vol. 2006, Article ID 78349, 16 pages, 2006.

[13] P. Zetterberg, "Wireless development laboratory (WIDELAB) equipment base," Tech. Rep. S3-SB-0316, Signals, Sensors and Systems (KTH), Stockholm, Sweden, August 2003, http://www.s3.kth.se.

[14] L. García-García, B. Lindmark, and C. Orlenius, "Design and evaluation of a compact antenna array for MIMO applications," in *Proceedings of IEEE Antennas and Propagation Society International Symposium*, pp. 313–316, Albuquerque, NM, USA, July 2006.

[15] B. Lindmark, N. Jaldén, P. Zetterberg, et al., "Antenna technology for reconfigurable multiple antenna terminals," Final Report WP 223, Antenna Center of Excellence (European Commission - 6th Framework Programme), Goteborg, Sweden, 2005, http://www.antennasvce.org.

[16] F. Adachi, M. T. Feeney, A. G. Williamson, and J. D. Parsons, "Crosscorrelation between the envelopes of 900 MHz signals received at a mobile radio base station site," *IEE proceedings*, vol. 133, no. 6, pp. 506–512, 1986.

[17] J. McFadden, "The correlation function of a sine wave plus noise after extreme clippings," *IEEE Transactions on Information Theory*, vol. 2, no. 2, pp. 82–83, 1956.

[18] J. N. Pierce and S. Stein, "Multiple diversity with nonindependent fading," *Proceedings of the IRE*, vol. 48, pp. 89–104, 1960.

[19] H. Özcelik, M. Herdin, W. Weichselberger, J. Wallace, and E. Bonek, "Deficiencies of 'Kronecker' MIMO radio channel model," *Electronics Letters*, vol. 39, no. 16, pp. 1209–1210, 2003.

[20] D. Chizhik, G. J. Foschini, and R. A. Valenzuela, "Capacities of multi-element transmit and receive antennas: correlations and keyholes," *Electronics Letters*, vol. 36, no. 13, pp. 1099–1100, 2000.

[21] M. Kassouf and H. Leib, "Shannon capacity and eigenbeamforming for space dispersive multipath MIMO channels," in *Proceedings of IEEE Wireless Communications and Networking (WCNC '03)*, vol. 1, pp. 156–161, New Orleans, La, USA, March 2003.